Journal of Thrombosis and Haemostasis, **7**: 2096–2105 DOI: 10.1111/j.1538-7836.2009.03640.x

ORIGINAL ARTICLE

Shear-induced unfolding activates von Willebrand factor A2 domain for proteolysis

C. BALDAUF,*†[1] R. SCHNEPPENHEIM,‡[1] W. STACKLIES,*† T. OBSER,‡ A. PIECONKA,§ S. SCHNEPPENHEIM,§ U. BUDDE,§ J. ZHOU*† and F. GRÄTER*†¶

**CAS-MPG Partner Institute for Computational Biology, Shanghai Institutes for Biological Sciences, Chinese Academy of Sciences, Shanghai, China; †EML Research, Heidelberg; ‡Department of Pediatric Hematology and Oncology, University Medical Center Hamburg-Eppendorf, Hamburg; §Coagulation Laboratory, AescuLabor Hamburg, Hamburg; and ¶Max-Planck-Institute for Metals Research, Stuttgart, Germany*

To cite this article: Baldauf C, Schneppenheim R, Stacklies W, Obser T, Pieconka A, Schneppenheim S, Budde U, Zhou J, Gräter F. Shear-induced unfolding activates von Willebrand factor A2 domain for proteolysis. *J Thromb Haemost* 2009; **7**: 2096–105.

Summary. *Background:* To avoid pathological platelet aggregation by von Willebrand factor (VWF), VWF multimers are regulated in size and reactivity for adhesion by ADAMTS13-mediated proteolysis in a shear flow dependent manner. *Objective and methods:* We examined whether tensile stress in VWF under shear flow activates the VWF A2 domain for cleavage by ADAMTS13 using molecular dynamics simulations. We generated a full length mutant VWF featuring a homologous disulfide bond in A2 (N1493C and C1670S), in an attempt to lock A2 against unfolding. *Results:* We indeed observed stepwise unfolding of A2 and exposure of its deeply buried ADAMTS13 cleavage site. Interestingly, disulfide bonds in the adjacent and highly homologous VWF A1 and A3 domains obstruct their mechanical unfolding. We find this mutant A2 (N1493C and C1670S) to feature ADAMTS13-resistant behavior *in vitro*. *Conclusions:* Our results yield molecular-detail evidence for the force-sensing function of VWF A2, by revealing how tension in VWF due to shear flow selectively exposes the A2 proteolysis site to ADAMTS13 for cleavage while keeping the folded remainder of A2 intact and functional. We find the unconventional 'knotted' Rossmann fold of A2 to be the key to this mechanical response, tailored for regulating VWF size and activity. Based on our model we discuss the pathomechanism of some natural mutations in the VWF A2 domain that significantly increase the cleavage by ADAMTS13 without shearing or chemical denaturation, and provide with the cleavage-activated A2 conformation a structural basis for the design of inhibitors for VWF type 2 diseases.

Keywords: ADAMTS13, force-probe molecular dynamics, Rossmann fold, shear flow, ultra-large von Willebrand factor.

Correspondence: Carsten Baldauf, CAS-MPG Partner Institute for Computational Biology, Shanghai Institutes for Biological Sciences, Chinese Academy of Sciences, 320 Yue Yang Road, 200031 Shanghai, China.
Tel.: +86 2154920475; fax: +86 2154920451.
E-mail: carsten@picb.ac.cn.

Reinhard Schneppenheim, Department of Pediatric Hematology and Oncology, University Medical Center Hamburg-Eppendorf, Martinistraβe 52, D-20246 Hamburg, Germany.
Tel.: +49 40428034270; fax: +49 40428034601.
E-mail: schneppenheim@uke.de.

Frauke Gräter, EML Research gGmbH – Villa Bosch, Schloss-Wolfsbrunnenweg 33, D-69118 Heidelberg, Germany.
Tel.: +49 6221533267; fax: +49 6221533298.
E-mail: frauke.graeter@eml-r.villa-bosch.de

[1]These authors contributed equally to this work.

Received 25 May 2009, accepted 16 September 2009

Introduction

von Willebrand factor (VWF) is a huge multimeric protein found in blood plasma. VWF mediates the adhesion of platelets to the sub-endothelial connective tissue and is the key protein in primary hemostasis in arterial vessels and the microcirculation [1,2]. Monomeric VWF is synthesized in megakaryocytes and endothelial cells. After transfer from the cytosol to the endoplasmatic reticulum, VWF matures by C terminal dimerization (disulfide bonds between CK domains) and N terminal multimerization (disulfide bonds between D3 domains) while being transferred through Golgi and post-Golgi apparatus. Finally stored in endothelial Weibel–Palade bodies and platelet α-granules, VWF is up to 100 monomers long and highly glycosylated [3]. Multimers are released from storage organelles by adequate stimuli.

The VWF multimers released from storage are particularly rich in ultra-large VWF (ULVWF). These highly active forms get rapidly yet only partially cleaved by the protease ADAMTS13 at the cleavage site Tyr1605–Met1606 within the A2 domain [4,5]. ADAMTS13 is a zinc-containing metalloprotease from the ADAMS/ADAMTS family. Shear stress in blood vessels has been shown to drive VWF multimers

into an elongated conformation with increased activity for adsorption to the blood vessel surface, a mechanism to stop bleeding after mechanical injury [6,7]. Mechanical forces due to shear flow regulate selective cleavage of ULVWF and thereby their size distribution [8,9]. If this size regulation fails, ULVWF accumulates and results in phenotypic manifestation of thrombotic thrombocytopenic purpura (TTP) [10]. In contrast, reduced VWF concentration, functional deficits, or complete absence of VWF results in the different types of von Willebrand disease (VWD) [11], the most common inherited bleeding disorder in humans. While the shear stress-induced adhesion and cleavage have been demonstrated in detail *in vitro*, the underlying molecular mechanism of shear-induced activation of VWF for ADAMTS13 cleavage is currently unknown.

Structural information in atomic detail for VWF is scarce. A single VWF is a multi-domain protein featuring a multitude of functionalities (Fig. 1A). The central A domain triplet is pivotal for adhesion and clotting, featuring binding sites for collagen (A1, A3) and the platelet receptor glycoprotein Ib (GPIb, A1), and the ADAMTS13 cleavage site (A2). A1 and A3 have been shown by X-ray crystallography [12,13] and A2 by homology modeling [14] and X-ray crystallography [15] to adopt a Rossmann α/β-fold. The ADAMTS13 cleavage site in A2 appears to be buried, suggesting that forces in stretched VWF multimers induce unfolding and exposure [16]. In recent experiments, described by the groups of Springer, Wong and co-workers [17], unfolding of the A2 domain by optical tweezers and subsequent cleavage by ADAMTS13 was observed.

We here investigate the unfolding and activation mechanism of A2 for ADAMTS13 cleavage under force by molecular simulations. By applying force distribution analysis, a method previously introduced by our group [18], we reveal how the atypical Rossmann fold topology of the VWF A2 domain senses mechanical force by selectively exposing and activating the ADAMTS13 cleavage site. We compare a homology model of the VWF A2 domain with the crystal structure 3GXB and discuss their special structural features. Furthermore, we predict and analyze, based on a homology model of the VWF A2 domain, the impact of mutations stabilizing the A2 domain by introducing a disulfide bond into VWF A2, in analogy with A1 and A3. We demonstrate this mutant VWF to be resistant against ADAMTS13 *in vitro*. Our results show VWF A2 domain unfolding as a response to shear stress to be the essential event in VWF size regulation.

Materials and methods

Homology modeling and in-silico mutation

The sequences of the VWF A domains have a residue identity of 20–25%. Based on multiple sequence alignments and structural alignments we created a homology model of the VWF A2 domain (residues 1488–1676 of human VWF) and

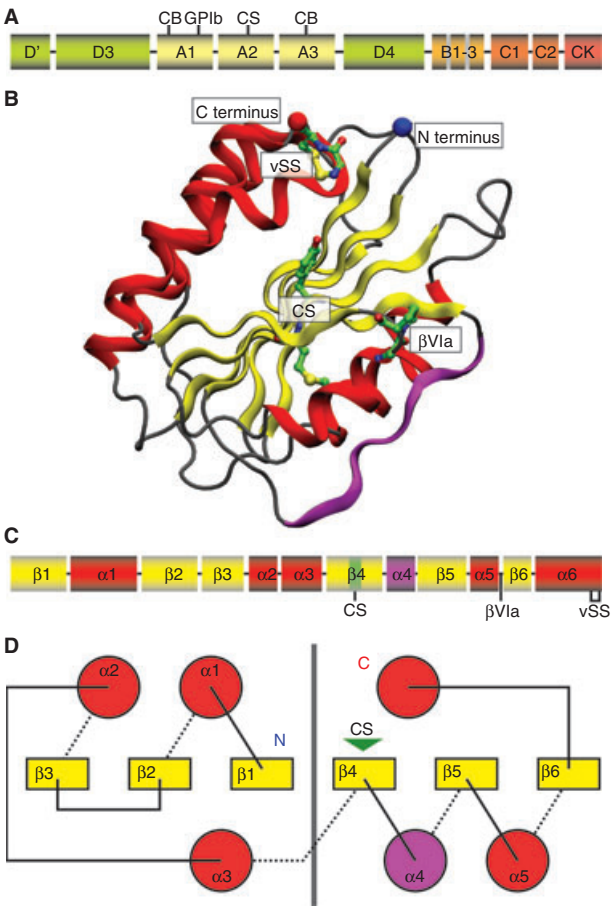

Fig. 1. (A) Domain organization of the VWF with collagen binding sites (CB) in domains A1 and A3, a glycoprotein Ib (GPIb) binding site in A3, and the ADAMTS13 cleavage site (CS) in A2. (B) Structure of the VWF A2 domain (PDB: 3GXB) in cartoon representation, the cleavage site (CS), the βVIa turn (βVIa), and the N terminal vicinal disulfide bridge (vSS) are highlighted in green; α-helices are red, β-sheets are yellow, and the α4-less loop is pink. (C) Secondary structure organization; β and α denote β-strand and α-helix, respectively. (D) The schematic sketch of the spatial secondary structure orientation shows the classical Rossmann fold of the C terminal half of the A2 domain with the cleavage site (CS, green marker) while the N terminal half shows a 'knotted' Rossmann fold with significantly higher stability under force.

the mutant A2 domain (N1493C and C1670S) from a human VWF A1 X-ray structure (PDB: 1AUQ). Details of the homology modeling performed with MOE (2007.9, Chemical Computing Group CCG, Montreal, Canada) can be found in the Supporting Information.

Based on the model of the A2 domain, the A2 double mutant N1493C/C1670S was generated. A disulfide bridge was introduced between the termini by the N1493C mutation, enabling a link between C1493 and C1669. To maintain a constant content of cysteine residues, known to be beneficial for protein expression (see below), a second mutation C1670S was introduced. Both models were validated by molecular dynamics (MD) simulation (Fig. S3B,C). The model is available as Supporting Information or from the authors.

Molecular dynamics simulation

All simulations and part of the analysis were carried out with the Gromacs suite of programs (version 3.3.1) [19]. The OPLS all-atom force field was used for the proteins [20] solvated in dodecahedral boxes with at least 7500 TIP4p water molecules [21], and periodic boundary conditions were applied. The typical protonation states at pH 7 were chosen for ionizable groups of the peptide. The necessary amount of counter-ions (Cl^- and Na^+) was added to ensure a neutral system. A temperature of 300 K and a pressure of 1 bar were assumed. The wild-type and mutant A2 models were simulated three times each for 30 ns and with different seeds for the initial velocity generation. Force-probe MD simulations, each ~26 ns in length, were performed two times independently on the 3GXB X-ray structure (residues 1495–1671) and three times independently on a truncated VWF A2 model (residues 1492–1670). Harmonic springs, attached to the terminal Cα atoms, with spring constants of 500 kJ $(\text{mol nm}^2)^{-1}$, were moved away from each other with a velocity of 1.25 nm ns^{-1}. To restrict the system size along the pulling direction, after partial unfolding the residues 1637–1671 of A2 (3GXB) and residues 1636–1670 of the A2 homology model were removed, water was added to the system, and the force-probe MD simulations were continued.

For FDA, two starting systems were taken from snapshots of the unfolding trajectory. Already unfolded parts, starting from Glu1652 for the first and from Ser1613 for the second system, were removed. Constant force of 10 and 100 pN, respectively, for the relaxed and stretched state, was applied in opposing direction to both termini. Each of the two systems was equilibrated under the respective constant force for 30 ns. For both systems, the all-atom RMSD to the starting structure remained below 0.35 nm for both pulling forces (Fig. S1), indicating that the system is able to bear the mechanical stress within this time scale without rupture. In the following, 10 simulations for the folded and 20 simulations for the unfolded state were performed for 30 ns and 15 ns each, starting with different random velocities. LINCS [22] and a time step of 2 fs were used for the folded state, whereas no constraints and a time step of 1 fs were used for the unfolded state. We used the FDA code [18] for Gromacs 4.0 [23] to write out forces F_{ij} between each atom pair i and j. Forces were averaged over the total simulation time of 300 ns per system, respectively, sufficient to obtain converged averages. Changes in forces, ΔF, are the differences in pair-wise forces between the systems pulled with 10 and 100 pN. Residue-wise forces F_{uv}^{res} were obtained by summing up forces F_{ij} for all pairs of atoms i and j in residues u and v, respectively. The absolute sum

$$\Delta F_u^{\text{res}} = \sum_v \left|\Delta F_{uv}^{\text{res}}\right|$$

reflects the changes in strain acting on a single residue and was used to color-code force distribution onto the protein backbone. Strain along the backbone was measured as the sum of all bonded interactions between adjacent residue pairs. As we use an approximation for angular and dihedral terms and solvent is not included in the FDA but in the simulations, changes in backbone forces indicate strain between two residues, but the values are not physically correct forces. Further simulation details can be found in the Supporting Information.

VWF engineering and analysis

By *in vitro* mutagenesis of full length VWF we exchanged N1493 at the N terminal site for cysteine and C1670, one of two neighboring cysteines at the C terminal site of the A2 domain, for serine to allow creation of a cysteine bond in the A2 domain. In additional mutagenesis experiments we also eliminated the existing disulfide bonds in the A1 (C1271S/D1459C) and A3 domains (C1686S/S1873C). *In vitro* mutagenesis of full length VWF cDNA in the mammalian expression vector pcDNA 3.1 was performed with the quick change mutagenesis kit (Stratagene) using primers of 41–46 bp in length harboring the particular base exchange. Transfer of the cDNA transfection of 293 cells by means of liposomal transfer, cell culture conditions, and harvesting and preparing of recombinant VWF, was performed as described previously [24]. The ADAMTS13 assay was based on recombinant human ADAMTS13 (rhuADAMTS13), adjusted to 0.05 U mL^{-1} in Tris/HCl buffer (5 mM, pH 8.0). 100 μL of this solution were added to 200 μL conditioned media containing rhuVWF (80 U dL^{-1}) and incubated with 10 mM barium chloride. The aliquots were then dialyzed against buffer solution (1.5 M urea, 5 mM Tris/HCl at pH 8.0) and incubated at 37 °C for 5h. The reaction was stopped with EDTA (10 mM) [24,25]. ADAMTS13-proteolyzed mutant and wild-type VWF was also analyzed by polyacrylamide gel electrophoresis under reducing conditions [26]. VWF phenotypic characterization by VWF multimer analysis recorded by digital photo imaging (FluorChem 8000) was carried out according to previously published protocols [27–29].

Results and discussion

Force-induced unfolding of the A2 domain

In vivo, the VWF multimer size is regulated by ADAMTS13 depending on shear flow conditions. Shear flow elongates VWF and results in a tensile force propagating throughout all VWF domains including A2 in the stretched protein [6,7]. We examined tensile stress on the VWF A2 conformation by force-probe MD simulations where a pulling force is applied on the termini of A2 in opposite directions. Force profiles for two independent simulations are shown in Fig. 2. The initial conformation (snapshot 1, Fig. 2) is stepwise unfolded. Starting from the C terminus the secondary structure elements are sequentially peeled-off, namely α6, β6 and α5 to yield a first intermediate (snapshot 3, Fig. 2), followed by β5 and the α4-less loop [15] leading to exposure of the cleavage site (snapshot 4, Fig. 2). Overall, inter-β

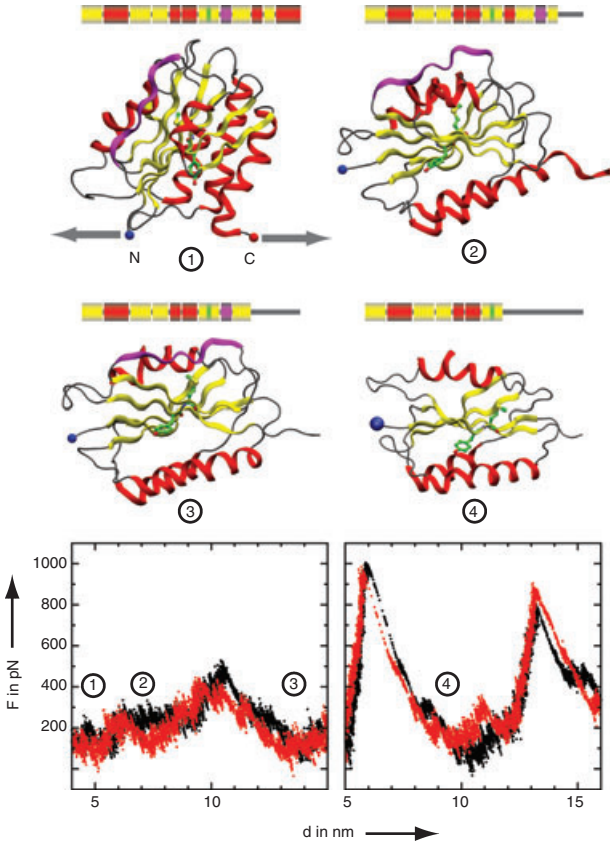

Fig. 2. The force profiles for two independent force-probe MD simulations of 3GXB are shown. After extending the protein chain to 15 nm, the simulations were continued with the unfolded C terminal part (sequence numbers 1637 and higher) being cut off. Selected snapshots are shown as cartoons; the cleavage site is shown in green; the fully unfolded C-terminal fragments in 2, 3 and 4 are omitted for clarity.

strand interactions show higher mechanical resistance than interactions involving helices. A short movie in the Supporting Information illustrates the sequential unfolding of VWF A2 under force.

In a very recent study, Wong, Springer and co-workers demonstrated the enforced activation of the VWF A2 domain for ADAMTS13 cleavage with a laser tweezers set-up [17]. They report a subset of their unfolding experiments to exhibit an intermediate state with a contour length of about 23 nm (40% of the length of the completely unfolded A2 domain with 58 ± 5 nm). Such an intermediate state corresponds well with the state 4 shown in Fig. 2. In this state 60 of 174 residues (35%) are unfolded at the C terminus, which results in an overall contour length of 24.6 nm, including the length of the intact N terminal part of the domain with 3 nm. Our force-probe simulations thus suggest that the experimentally detected unfolding intermediate is ready for cleavage by ADAMTS13. A study by De Cristofaro and co-workers is focused on the mechanism of ADAMTS13 catalysis. Their work with VWF73 (a truncated A2 domain covering VWF residues Asp1596–Arg1668) suggests as well that a partially unfolded state of VWF A2 is ready for ADAMTS13 cleavage [30].

Force distribution analysis of the VWF A domain

The stable N terminal β1 strand is locked to the center of the protein, keeping the protein core including the cleavage site largely intact (Fig. 1D), while the C terminal structural elements, being more responsive to the external force, are pulled out step by step until the cleavage site is accessible. This distinct response of the two halves of the domain is determined by the underlying topology of the VWF A-type domains. The C terminal part of the A2 domain represents a Rossmann fold,

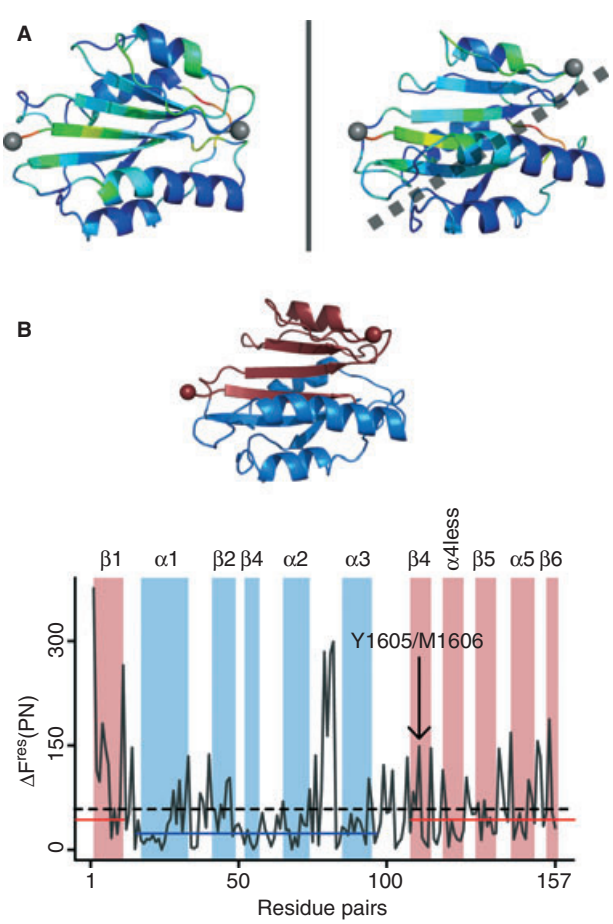

Fig. 3. Force distribution analysis (FDA) of the A2 domain (3GXB). (A) Cartoon representation of an A2 folded state (state 2 in Fig. 2) in two views. Changes in pair-wise forces, ΔF, are color-coded ranging from blue for ΔF = 0 to red for high ΔF. The external pulling force distributes along a direct path between termini, leaving the N-terminal part nearly unaffected (below the dotted line). (B) Strain along the backbone of the folded structure (solid gray line), measured in terms of changes in bonded interactions between residue pairs. Sequence positions of secondary structure elements (helices and strands) are highlighted by colored bars. The color-coding reflects the protein topology: structural elements that are unfolded in state 4 of Fig. 2 and strand β1 are red; structural elements that remain intact in state 4 of Fig. 2 are blue (compare with the cartoon representation above the plot). The dashed line represents the mean force over all bonded residue pairs. This mean force on structural elements α1, β2, β3, α2 and α3 (blue line) is lower than on structural elements β1, β4, α4less, β5, α5 and β6 (red line). High pair-wise forces around Thr1576 (between α2 and α3) are an artifact resulting from rare loop rearrangements.

with the characteristic sequential order of the secondary structure elements β4–α4 less–β5–α5–β6–α6, bridging each strand in the parallel β sheet alignment with an α helix (Fig. 1D). This sequential arrangement results in the stepwise unfolding under force. In contrast, the modified Rossmann fold of the N terminal half of the A2 domain prevents unfolding. Here, β strands are swapped such that β1, the strand directly subjected to the external force, is tightly embedded in the protein core (Fig. 1D), so as to form rupture-resistant interactions with adjacent strands β2 and β4.

We further validated the key role of this particular 'knotted' Rossmann topology for the mechanical response of A2 by force distribution analysis (FDA). FDA reveals the distribution of internal strain within a structure subjected to an external force by monitoring changes in pair-wise atomic forces ΔF [18]. We determined the strain distribution in an early unfolding intermediate of the VWF A2 domain in which the mechanically labile helix α6 is already unraveled (Fig. 2, snapshot 2). The tensile force mainly propagates through the part of the central β sheet formed by strands 1, 4, 5 and 6 of the domain (Fig. 3A), following a direct path between the two termini. Force distributes from the C terminal strand via strands β5 and β4 to the very center of the structure, strand β1, transferring the force out of the domain to the N terminus. From the pair-wise forces plotted in Fig. 3(B) it is also evident that substantial parts of the N terminal half are under low (sub-average) force as a direct result of the unconventional Rossmann fold. Significant high forces in this part of the protein are only observed at the loop directly attached to strand β1 (connection to helix α1) and at the loop connecting α1 and β2, that is in close proximity to the N terminus, the point of force application. Strand β1 virtually shields the tertiary structure formed by β1–α1–β2–β3–α2–α3 from force-induced unfolding. Accordingly, this area is under low strain, as evident by the cold coloring mapped on the structure in Fig. 3A. The shielded region is in the lower right of the dashed line. Interestingly, this architecture would allow the N terminal half of the A2 domain to carry out a particular – albeit currently unknown – function, even while the C terminus is unfolded and cleavage ready.

The cleavage site Tyr1605–Met1606 is the topological middle point of the folded and intact A2 domain and therewith protected from cleavage. Mechanical force induced a cleavage-ready unfolding intermediate as observed in our force-probe MD simulation (Fig. 2 state 4) as well as in experiments [17]. In order to investigate the impact of pulling forces on the cleavage site, the Tyr1605–Met1606 peptide bond, FDA was performed on the partially unfolded cleavage-ready A2 domain. We find the backbone between Tyr1605 and Met1606 to be under extra-ordinarily high strain, and strain distribution seems to be directed in a way to specifically target these residues, Fig. 4A. Analysis of inter-side chain forces, this is, forces that pairs of side chains exert on each other, reveals that a large part of the strain on the cleavage site results from neighboring residues located in the central β-strands. The force network in Fig. 4(B), mapping changes in forces between residue pairs as edges onto the structure, shows a clear polarization. There are almost no edges crossing a virtual plane that separates the cleavage site residues, resulting in a weakened peptide bond potentially mechanically activated for cleavage. This specific deflection of mechanical load onto the cleavage site is mainly realized by strong pair-wise interactions between Tyr1605 and Ala1500, Phe1501, Val1502 and Val1604 (Fig. 4C), and between Met1606 and Thr1608 (Fig. 4D), respectively. Thus, in addition to mere exposure to ADAMTS13, the Tyr1605–Met1606 proteolytic site in the VWF A2 unfolding intermediate is selectively tensed up due to an optimized force distribution. We therefore predict mutations in the local force network to attenuate the strain in the peptide bond and to consequently alter its susceptibility to ADAMTS13 cleavage.

Homology modeling of the VWF A2 domain

Until recently [15], no experimentally derived structural data on the VWF A2 domain was available. Thus, a homology model including residues 1488–1676 of human VWF was created. The model fully includes the very terminal sequences of A2, and thereby the site of mutagenesis for introducing a disulfide bond (see below). It is therefore more comprehensive but otherwise highly similar to a previous homology model that covers only the VWF residues 1496–1669 [14] and to the X-ray structure 3GXB covering residues 1495 to 1671 (Fig. S4) [15]. The rmsd (N, Cα, Cβ, C, O) between snapshots of our trajectories of the homology model and 3GXB is around 0.2 nm, and < 0.1 nm for the heavy atoms of the cleavage site. Also, the unfolding mechanism of A2 observed in our simulations largely agrees with the X-ray structure and the model (cf. Fig. 2 and Fig. S5). The predictability of the A2 structure, including differences in A1 and A3, implies that the tertiary fold is largely defined by the primary sequence of A2. However, our model also misses two features by which A2 differs from its highly related adjacent domains, as now revealed by the A2 crystal structure [15] (cf. Fig. S4):

First, the remarkable experimental finding of a vicinal disulfide bridge between the very terminal Cys residues 1669 and 1670 was not predicted in the homology model. Helix α6 is capped and rigidified by the C terminal vicinal disulfide bond, thereby mechanically stabilized and unfolding at once. With reduced Cys side chains as in our homology model, the helix unfolds stepwise in the force-probe simulations (Fig. S5). The presence of the helix cap, however, does not significantly change the rate limiting steps involving high forces for the rupture of the hydrogen network of the central β-sheet after the early helix α6 unfolding. Based on the high strain of the eight-membered disulfide-bonded ring and possible environmental changes, we hypothesize a redox-dependent regulation of the forced onset of A2 unfolding via the vicinal disulfide bond.

Second, the peptide bond between Trp1644 and Pro1645 is *cis* configured in the X-ray structure. The turn comprising this peptide bond is of type βVIa [31] in the X-ray structure, while a

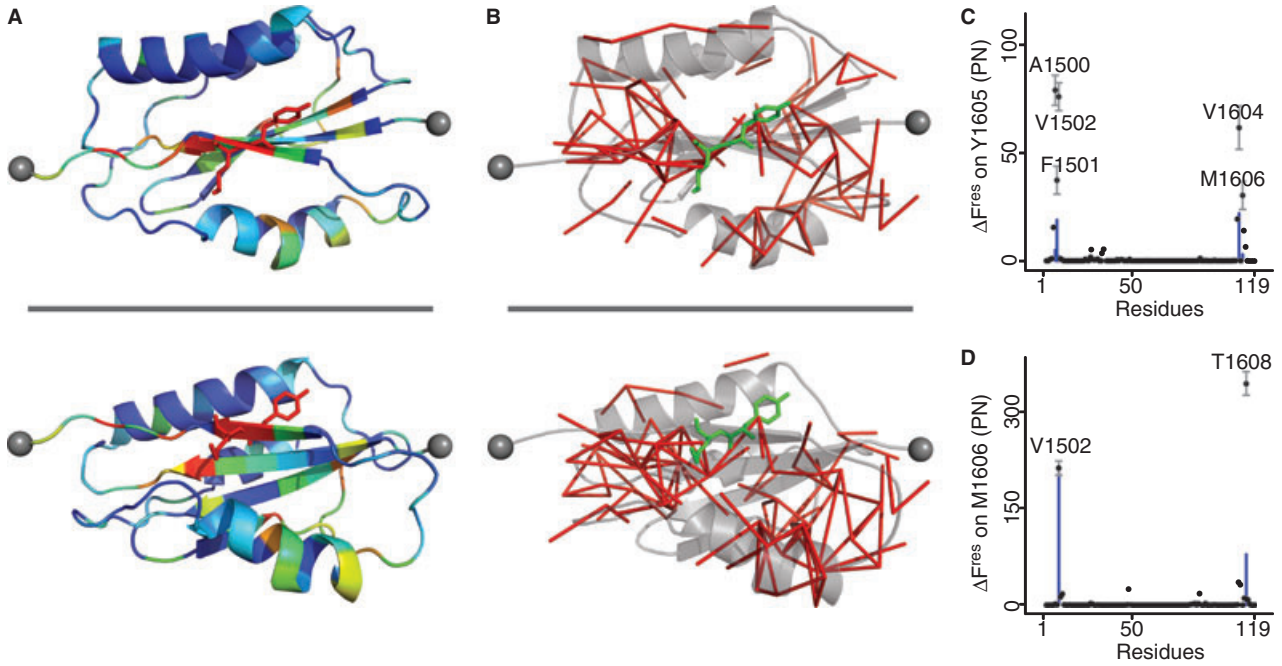

Fig. 4. Force distribution analysis (FDA) of the partially unfolded A2 domain (3GXB). (A) Cartoon representation of the cleavage-ready A2 unfolding intermediate (compare state 4 in Fig. 2). Backbone strain, measured in terms of changes in pair-wise forces, ΔF, is color coded onto the structure, with colors ranging from blue for ΔF = 0 to red for high ΔF. The cleavage site (sticks) exhibits particularly high strain. Helices α1 to α4 are not under strain. (B) Graph-like representation of force distribution in the cleavage-ready A2 unfolding intermediate. Edges represent changes in forces between residue pairs that exceed a threshold of 30 pN. (C) Strain induced on the cleavage site residue Y1605 by adjacent residues. The plot shows changes in inter-residue forces ΔF^{res} for Y1605; the contribution of the Y1605 side-chain is plotted as straight blue lines. Standard errors are plotted as whiskers. (D) Same as (C) but for M1606.

βIII turn is predicted in our model instead (cf. Fig. S4). Our A2 model suggests that *cis* as well as *trans* configuration for this particular peptide bond is structurally feasible. Given the impact of *cis-trans* isomers on protein folding [32], their possible interconversion by mechanical forces [33], and the absence of Prolyl-*cis*/*trans*-isomerases in the extra-cellular space, they might play a regulatory role.

However, the actual physiological significance of both, the vicinal disulfide bridge and the *cis* or *trans* configuration of the peptide bond, remains to be identified for this particular case.

In vitro *mutagenesis and electrophoretic analysis*

Our unfolding simulations suggest A2 to be activated for ADAMTS13 cleavage under high shear flow conditions by exposing the cleavage site after partial unfolding of the C-terminal domain. A1 and A3 have highly similar amino acid sequences and three-dimensional structures, and thus would be expected to unfold along a similar mechanism. Examination of the 3D structures of the VWF A domains shows the existence of disulfide linkages between the termini of the A1 and A3 domains, respectively, but not for the A2 domain. The snipped sequence alignment in Fig. 5A illustrates that A1 and A3 feature two cysteine residues each at their N and C termini, allowing the formation of disulfide bridges. A2 has two vicinal cysteine residues at its C terminus (Fig. 5A) and none at the N terminus. The domain can unfold under force and is mechano-responsive. The cysteine hooks ensure the structural integrity of A1 and A3 under shear flow for specific interactions with collagen and GPIb as essential for VWF adhesion and aggregation, while allowing the selective force-induced unfolding of only the A2 domain for cleavage by ADAMTS13.

Based on the homology model of the VWF A2 domain, we designed the ADAMTS13-resistant VWF variant mutA2 (cf. Table 1 for nomenclature of all VWF variants) by introducing a cysteine at position N1493 to allow disulfide bond formation with residue C1669 at the A2 C-terminus in analogy with the A1 domain. The magnification in Fig. 5A illustrates the virtually perfect orientation of the side chains of residues N1493 and C1669. C1670 was changed to serine to generate maximal homology of A2 with A1 and A3 and to avoid the possibility of alternate disulfide bonding at the A2 carboxy terminal. A model of the mutant A2 domain was subjected to MD simulations to test the feasibility of disulfide bond formation and the domain's structural integrity upon mutation. The data are shown in the Supporting Information (Fig. S3C) and indicate tolerance of the mutations and conservation of the A2 structural features.

To confirm the generation of an artificially introduced A2 disulfide bond *in vitro*, we subjected A2 mutant full-length recombinant VWF (mutA2) to multimer analysis in

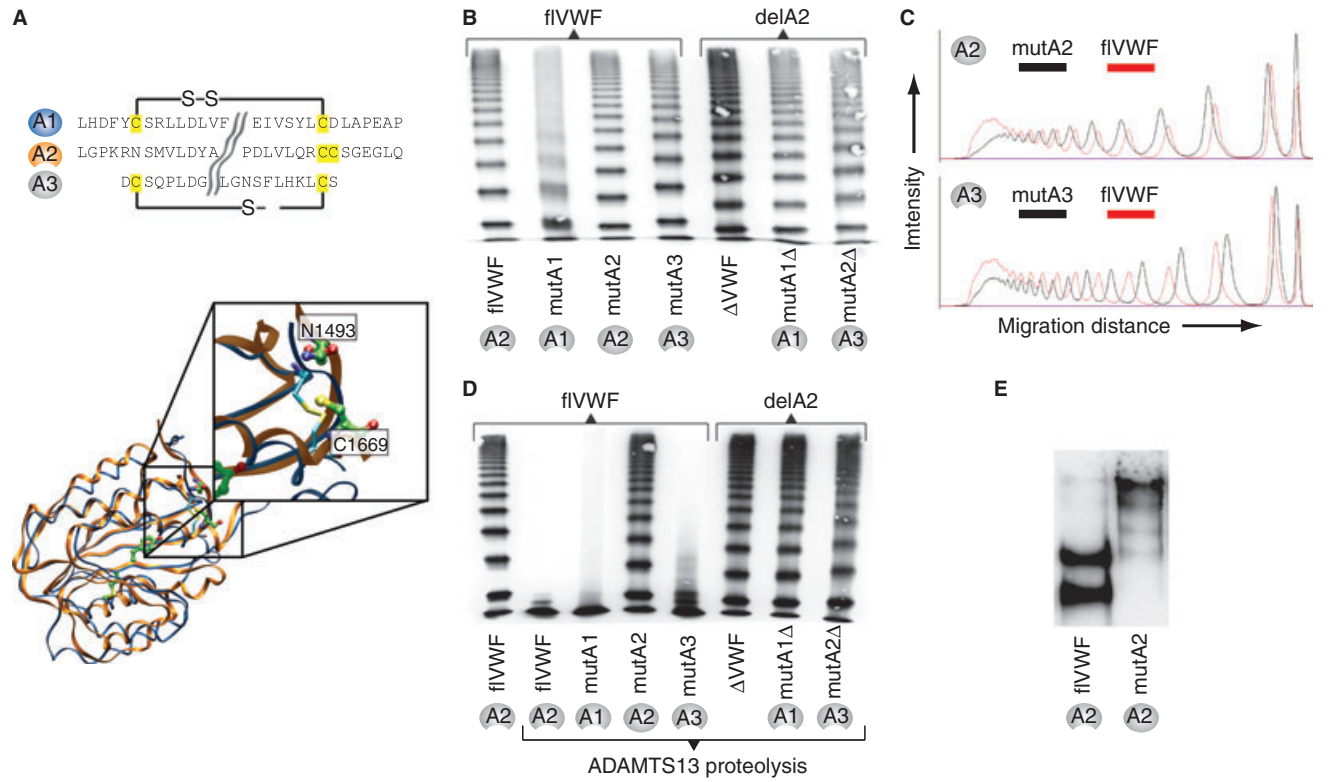

Fig. 5. (A) The A1 domain (blue ribbons and blue carbon atoms) is locked by a disulfide bond between the termini, while the A2 domain (orange ribbons and green atoms) lacks this feature. Mutation N1493C would allow disulfide bond formation (magnification). In the schematic sequence alignment of the VWF A domains only the N- and C-terminal sequences are shown (see Supporting Information for full alignment), cysteine residues are highlighted and disulfide bonds are shown as brackets. Closed circles indicate disulfide linkage of the domain termini; open circles indicate no disulfide linkage of the domain termini. (B) Electrophoretic multimer analysis of VWF variants. Downwards shifted bands indicate faster migration (mutA2) compared with flVWF, while upwards shifted bands indicate slower migration (mutA1 and mutA3). (C) Scan of selected lanes of the gel shown in Fig. 5(B): the shift of bands relative to flVWF multimers indicates faster migration of mutA2 and slower migration of mutA3. (D) ADAMTS13 proteolysis of VWF variants monitored by electrophoresis. Normal proteolysis is observed for flVWF, mutA1 and mutA3, whereas proteolysis is absent in all other variants including mutA2. (E) Full-length A2 domain mutant mutA2 in comparison with flVWF after ADAMTS13 treatment and reduction of disulfide bonds. Wild-type VWF is proteolyzed completely and displays the expected two proteolytic fragments after reduction, whereas mutA2 is not proteolysed.

Table 1 Overview of the expressed VWF variants, their sensitivity against ADAMTS13 and the relative migration speed of the multimers in electrophoresis

Name	Mutations	Cleavage by ADAMTS13	Migration relative to flVWF
Based on full-length VWF			
flVWF	None	+	–
mutA1	C1272S/D1459C	+	Slower
mutA2	N1493C/C1670S	–	Faster
mutA3	C1686S/S1873C	+	Slower
Based on VWF without A2 domain			
ΔVWF	None	–	–
mutA1Δ	C1272S/D1459C	–	–
mutA3Δ	C1686S/S1873C	–	–

comparison with flVWF. The mutA2 variant migrated faster than flVWF, suggesting a more compact structure with higher electrophoretic mobility (Fig. 5B,C). In contrast, removing the disulfide bridges in the A1 (C1272S and D1459C, mutA1) or A3 domain (C1686S and S1873S, mutA3) towards an open structure as in wild-type A2 resulted in a decrease of the electrophoretic mobility, both in the presence and absence of A2, respectively (Fig. 5B,C). These results support the assumption of the generation of a cysteine-bridge connection of the A2 N and C terminus analogous to A1 and A3. We then exposed all variants to ADAMTS13 and monitored proteolysis by multimer analysis. We could show that, in contrast to flVWF, ADAMTS13 proteolysis of mutA2 was completely absent, similar to the A2 domain deleted VWF variants ΔVWF, mutA1Δ and mutA3Δ (Fig. 5D). This was further confirmed by reduction of cysteine bonds by β-mercaptoethanol to exclude the possibility that the mutA2 variant was actually proteolysed but just held together by the created cysteine bonds (Fig. 5E). Opening the disulfide bond of the A1 and A3 domain by mutagenesis in A2 domain deleted VWF (variants mutA1D and mutA3D) did not result in proteolytic susceptibility of the respective domains, indicating that the homology of A1 and A3 to A2 is too low for substrate recognition by ADAMTS13 (Fig. 5D). A speculative physiological

effect of the loss of the termini-linking disulfide bonds in A1 and A3 domain would suggest a significantly reduced affinity of A1 to collagen and GPIb and of A3 to collagen due to the disturbed structural integrity, especially in blood flow.

Conclusions

We here show by simulations and *in vitro* mutagenesis how force-induced partial unfolding is required for ADAMTS13-mediated cleavage of VWF A2. The unfolding and activation mechanism of A2 can be abolished by a single mutation, N1493C, in analogy with the mechanism that presumably protects A1 and A3 from unfolding and loss of function. We find the C-terminal part of VWF A2 to be unraveled under force, suggesting ADAMTS13 to primarily recognize this partially unfolded domain rather than the native state of A2. This is in excellent agreement with recent *in vitro* studies on the interaction of VWF A2 with ADAMTS13 [34,35]. Our data also suggest that this ADAMTS13-susceptible unfolding intermediate corresponds to the intermediate very recently observed in A2 single molecule stretching experiments [17].

The force-sensing mechanism of the A2 domain provides an intriguing explanation for the size regulation of ULVWF: larger multimers involve higher pulling forces and therefore higher unfolding rates at a given shear flow. As a result, larger VWF is cleaved more readily. The forces required for the exposure of the cleavage site in A2 as observed here (up to 1000 pN) can be expected to be significantly larger than those inducing unfolding in *in vivo* conditions due to the short nanosecond time scale of the simulations within which the unfolding is forced to occur [36]. Under physiological conditions, cleavage will preferentially occur for the upper limit of VWF multimer sizes, and thus under flow conditions that lead to tensile forces beyond the 5–10 pN estimated for average VWF sizes [6] (A Alexander-Katz, personal communication, 2009). Indeed, the experimental evaluation of VWF A2 unfolding by optical tweezers suggests forces in the range of 10–15 pN [17].

The intermediates of mechanical unfolding of the VWF A2 domain observed here (and not a static intact equilibrium state) represent the substrate of ADAMTS13. These dynamics of the A2 domain during unfolding are prerequisite to explore the structural and functional determinants of A2 recognition by ADAMTS13. The gained knowledge (e.g. the actual structure of the partially unfolded A2 domain) can be used to design inhibitors of ADAMTS13 and can provide a route to drugs targeting enhanced VWF cleavage in blood.

VWF A2 mutations previously identified as causing von Willebrand disease type IIA due to an increased susceptibility to ADAMTS13 [24] cleavage can now be rationalized on the basis of our model. They can be expected to involve destabilization of the overall A2 structure by forcing charged groups into regions of hydrophobic packing (I1628T and G1629E), perturbing β-turn formation between the VWF A2 secondary structure elements β5 and α5 (G1631D), or by destabilizing A2 due to a drastic increase in spatial demand of the side chain (G1609R). Structural destabilization in turn facilitates A2 unfolding and cleavage site exposure to ADAMTS13.

While the C terminal part of the A2 domain follows a highly conserved unfolding pattern if subjected to tensile stress, the N terminal 'knotted' Rossmann fold remains completely intact even under high forces. We hypothesize that the second important function of A2, the proposed inhibition of the A1 GPIb interaction [37], which mediates the binding of VWF to platelets, is located at this force-resistant part of the domain. Thereby, as a consequence of the two distinct Rossmann topologies within the A2 domain, size regulation of VWF by ADAMTS13 does not affect platelet interaction. As a second consequence of the unconventional Rossmann fold, we find strain to internally propagate selectively to the ADAMTS13 cleavage site, bringing the peptide bond under tension. We hypothesize that this specific force-activation affects the catalytic activity of ADAMTS13, as a direct impact of the A2 mechanics on the A2-ADAMTS13 biochemistry, similar to what has been shown for disulfide bond cleavage by DTT and thioredoxin [38].

We here assumed that the stretching force in VWF propagates to A2 primarily along the protein backbone. A full A1-A2-A3 structure is needed to re-examine the unfolding mechanism taking inter-domain interactions into account, as a next important step towards deciphering the molecular details of VWF mechanical response.

Another example for a Rossmann fold in which the termini are locked together by a disulfide bond is the VWF type A domain of human capillary morphogenesis protein 2, interestingly again a collagen-binding adhesion protein [39]. To what extent nature has made use of the Rossmann fold as a module that can be reversibly switched into a force-resistant state remains to be seen.

Addendum

C. Baldauf, R. Schneppenheim and F. Gräter designed the research described in this article. C. Baldauf, W. Stacklies and J. Zhou performed modeling and simulation described in the article. T. Obser, A. Pieconka and S. Schneppenheim performed experiments. C. Baldauf, R. Schneppenheim, W. Stacklies and U. Budde analyzed and interpreted the data. C. Baldauf, R. Schneppenheim, W. Stacklies and F. Gräter wrote the paper.

Acknowledgements

The authors thank M. F. Schneider and A. Alexander-Katz for fruitful discussions and W. Wong and T. Springer for early communication of their findings. CB thanks R. Meier and W. Sippl (Institute of Pharmaceutical Chemistry, Martin-Luther University of Halle-Wittenberg) for the possibility of a research

stay and for help with the creation of the homology model. CB and FG thank Y. Yin for performing structure searches. CB is grateful for a Feodor Lynen Fellowship by the Alexander von Humboldt foundation.

Disclosure of Conflict of Interests

The authors state that they have no conflict of interests.

Supporting Information

Additional Supporting Information may be found in the online version of this article:

Figure S1. (A) Superposition of the average structures under 10 and 100 pN in the folded state used for FDA. Structures are averages over 300 ns, respectively. (B) Superposition of the average structures under 10 and 100 pN of the unfolding intermediate. Structures are averages over 300 ns, respectively.
Figure S2. Multiple sequence alignment used as basis for homology modeling.
Figure S3. (A) Verification of the Homology Model with ProSA 2003: The energy analysis is smoothed with a window size of 30 aa. Characterizing the model with ProSA-Web shows a Z-score for the raw model of -6.99, and of -8.11 for the model after 10 ns MD simulation. The Z-score for the structure model published by Sutherland et al. is -7.84. (B) Backbone rmsd of the wild type A2 domain monitored in three independent 30 ns MD simulations. (C) Backbone rmsd of the mutant A2 (N1493C/C1670S) domain monitored in three independent 30 ns MD simulations.
Figure S4. Superposition of 3GXB (silver) and the homology model (orange), the main chain RMSD is 0.189 nm.
Figure S5. The force profiles for three independent force-probe MD simulations of our VWF A2 domain model.
Dataset S1. Homology model of the A2 domain including VWF residues 1488 to 1676 in PDB-format.
Video S1. Visualization of a VWF A2 Domain Force Probe MD Simulation.

Please note: Wiley-Blackwell are not responsible for the content or functionality of any supporting materials supplied by the authors. Any queries (other than missing material) should be directed to the corresponding author for the article.

References

1 Sadler JE. New concepts in von Willebrand disease. *Annu Rev Med* 2005; **56**: 173–91.
2 Ruggeri ZM. The role of von Willebrand factor in thrombus formation. *Thromb Res* 2007; **120**: S5–9.
3 Millar CM, Brown SA. Oligosaccharide structures of von Willebrand factor and their potential role in von Willebrand disease. *Blood Rev* 2006; **20**: 83–92.
4 Dent JA, Berkowitz SD, Ware J, Kasper CK, Ruggeri ZM. Identification of a cleavage site directing the immunochemical detection of molecular abnormalities in type IIa von Willebrand-factor. *Proc Natl Acad Sci USA* 1990; **87**: 6306–10.
5 Sadler JE. A new name in thrombosis, ADAMTS13. *Proc Natl Acad Sci USA* 2002; **99**: 11552–4.
6 Alexander-Katz A, Schneider MF, Schneider SW, Wixforth A, Netz RR. Shear-flow-induced unfolding of polymeric globules. *Phys Rev Lett* 2006; **97**: 138101.
7 Schneider SW, Nuschele S, Wixforth A, Gorzelanny C, Alexander-Katz A, Netz RR, Schneider MF. Shear-induced unfolding triggers adhesion of von Willebrand factor fibers. *Proc Natl Acad Sci USA* 2007; **104**: 7899–903.
8 Perutelli P, Amato S, Molinari AC. ADAMTS-13 activity in von Willebrand disease. *Thromb Res* 2006; **117**: 685–8.
9 Shida Y, Nishio K, Sugimoto M, Mizuno T, Hamada M, Kato S, Matsumoto M, Okuchi K, Fujimura Y, Yoshioka A. Functional imaging of shear-dependent activity of ADAMTS13 in regulating mural thrombus growth under whole blood flow conditions. *Blood* 2008; **111**: 1295–8.
10 Sadler JE. Von Willebrand factor, ADAMTS13, and thrombotic thrombocytopenic purpura. *Blood* 2008; **112**: 11–8.
11 Von Willebrand EA. Hereditar pseudohemofili. *Fin Lakaresallsk Handl* 1926; **68**: 7–112.
12 Emsley J, Cruz M, Handin R, Liddington R. Crystal structure of the von Willebrand factor A1 domain and implications for the binding of platelet glycoprotein Ib. *J Biol Chem* 1998; **273**: 10396–401.
13 Huizinga EG, van der Plas RM, Kroon J, Sixma JJ, Gros P. Crystal structure of the A3 domain of human von Willebrand factor: implications for collagen binding. *Structure* 1997; **5**: 1147–56.
14 Sutherland JJ, O'Brien LA, Lillicrap D, Weaver DF. Molecular modeling of the von Willebrand factor A2 domain and the effects of associated type 2A von Willebrand disease mutations. *J Mol Model* 2004; **10**: 259–70.
15 Zhang Q, Zhou Y-F, Zhang C-Z, Zhang X, Lu C, Springer TA. Structural specializations of A2, a force-sensing domain in the ultralarge vascular protein von Willebrand factor. *Proc Natl Acad Sci USA* 2009; **106**: 9226–31.
16 Dong JF, Moake JL, Nolasco L, Bernardo A, Arceneaux W, Shrimpton CN, Schade AJ, McIntire LV, Fujikawa K, Lopez JA. ADAMTS-13 rapidly cleaves newly secreted ultralarge von Willebrand factor multimers on the endothelial surface under flowing conditions. *Blood* 2002; **100**: 4033–9.
17 Zhang XH, Halvorsen K, Zhang CZ, Wong WP, Springer TA. Mechanoenzymatic cleavage of the ultralarge vascular protein von Willebrand factor. *Science* 2009; **324**: 1330–4.
18 Stacklies W, Vega MC, Wilmanns M, Gräter F. Mechanical network in titin immunoglobulin from force distribution analysis. *PLoS Comput Biol* 2009; **5**: e1000306.
19 Lindahl E, Hess B, Van der Spoel D. GROMACS 3.0: a package for molecular simulation and trajectory analysis. *J Mol Model* 2001; **7**: 306–17.
20 Jorgensen WL, Ulmschneider JP, Tirado-Rives J. Free energies of hydration from a generalized Born model and an ALL-atom force field. *J Phys Chem B* 2004; **108**: 16264–70.
21 Lawrence CP, Skinner JL. Flexible TIP4P model for molecular dynamics simulation of liquid water. *Chem Phys Lett* 2003; **372**: 842–7.
22 Hess B, Bekker H, Berendsen HJC, Fraaije J. LINCS: a linear constraint solver for molecular simulations. *J Comput Chem* 1997; **18**: 1463–72.
23 Hess B, Kutzner C, van der Spoel D, Lindahl E. GROMACS 4: Algorithms for highly efficient, load-balanced, and scalable molecular simulation. *J Chem Theory Comput* 2008; **4**: 435–47.
24 Hassenpflug WA, Budde U, Obser T, Angerhaus D, Drewke E, Schneppenheim S, Schneppenheim R. Impact of mutations in the von Willebrand factor A2 domain on ADAMTS 13-dependent proteolysis. *Blood* 2006; **107**: 2339–45.
25 Furlan M, Robles R, Lammle B. Partial purification and characterization of a protease from human plasma cleaving von Willebrand factor to fragments produced by in vivo proteolysis. *Blood* 1996; **87**: 4223–34.

26 Schneppenheim R, Brassard J, Krey S, Budde U, Kunicki TJ, Holmberg L, Ware J, Ruggeri ZM. Defective dimerization of von Willebrand factor subunits due to a Cys- > Arg mutation in type IID von Willebrand disease. *Proc Natl Acad Sci USA* 1996; **93**: 3581–6.
27 Budde U, Schneppenheim R, Eikenboom J, Goodeve A, Will K, Drewke E, Castaman G, Rodeghiero F, Federici AB, Batlle J, Perez A, Meyer D, Mazurier C, Goudemand J, Ingerslev J, Habart D, Vorlova Z, Holmberg L, Lethagen S, Pasi J, *et al*. Detailed von Willebrand factor multimer analysis in patients with von Willebrand disease in the European study, molecular and clinical markers for the diagnosis and management of type 1 von Willebrand disease (MCMDM-1VWD). *J Thromb Haemost* 2008; **6**: 762–71.
28 Ruggeri ZM, Zimmerman TS. The complex multimeric composition of factor-VIII-von Willebrand factor. *Blood* 1981; **57**: 1140–3.
29 Schneppenheim R, Plendl H, Budde U. Luminography – an alternative assay for detection of von Willebrand factor multimers. *Thromb Haemost* 1988; **60**: 133–6.
30 Di Stasio E, Lancellotti S, Peyvandi F, Palla R, Mannucci PM, De Cristofaro R. Mechanistic studies on ADAMTS13 catalysis. *Biophys J* 2008; **95**: 2450–61.
31 Möhle K, Gussmann M, Hofmann H-J. Structural and energetic relations between beta turns. *J Comput Chem* 1997; **18**: 1415–30.
32 Fischer G. Chemical aspects of peptide bond isomerisation. *Chem Soc Rev* 2000; **29**: 119–27.
33 Valiaev A, Lim DW, Oas TG, Chilkoti A, Zauscher S. Force-induced prolyl cis-trans isomerization in elastin-like polypeptides. *J Am Chem Soc* 2007; **129**: 6491–7.
34 Wu JJ, Fujikawa K, McMullen BA, Chung DW. Characterization of a core binding site for ADAMTS-13 in the A2 domain of von Willebrand factor. *Proc Natl Acad Sci USA* 2006; **103**: 18470–4.
35 Gao WQ, Anderson PJ, Sadler JE. Extensive contacts between ADAMTS13 exosites and von Willebrand factor domain A2 contribute to substrate specificity. *Blood* 2008; **112**: 1713–9.
36 Evans E, Ritchie K. Dynamic strength of molecular adhesion bonds. *Biophys J* 1997; **72**: 1541–55.
37 Martin C, Morales LD, Cruz MA. Purified A2 domain of von Willebrand factor binds to the active conformation of von Willebrand factor and blocks the interaction with platelet glycoprotein Ib alpha. *J Thromb Haemost* 2007; **5**: 1363–70.
38 Wiita AP, Perez-Jimenez R, Walther KA, Grater F, Berne BJ, Holmgren A, Sanchez-Ruiz JM, Fernandez JM. Probing the chemistry of thioredoxin catalysis with force. *Nature* 2007; **450**: 124–7.
39 Lacy DB, Wigelsworth DJ, Scobie HM, Young JAT, Collier RJ. Crystal structure of the von Willebrand factor A domain of human capillary morphogenesis protein 2: an anthrax toxin receptor. *Proc Natl Acad Sci USA* 2004; **101**: 6367–72.